Earth and Planetary Science Letters 408 (2014) 146–154

Contents lists available at ScienceDirect

Earth and Planetary Science Letters

www.elsevier.com/locate/epsl

Permeability of the Lucky Strike deep-sea hydrothermal system: Constraints from the poroelastic response to ocean tidal loading

Thibaut Barreyre [a,b,*], Javier Escartin [a], Robert Sohn [b], Mathilde Cannat [a]

[a] Institut de Physique du Globe de Paris, CNRS, UMR 7154, Paris Cedex 5, France
[b] Woods Hole Oceanographic Institution, Woods Hole, MA, USA

ARTICLE INFO

Article history:
Received 19 May 2014
Received in revised form 29 September 2014
Accepted 30 September 2014
Available online 27 October 2014
Editor: P. Shearer

Keywords:
poroelasticity
tidal loading
permeability
deep-sea hydrothermal field
spectral analysis
temperature time-series

ABSTRACT

We use the time delay between tidal loading and the induced subsurface flow response to constrain the poroelastic behavior and permeability of the Lucky Strike hydrothermal field on the Mid-Atlantic Ridge. We demonstrate that high-temperature ($T > 200\,^{\circ}C$) exit-fluid discharge records from four hydrothermal sites across the field are highly coherent with contemporaneously acquired bottom pressure records at tidal periods, with the thermal response lagging pressure by ~155° (5.3 h) on average across all sites for the semi-diurnal (M2) frequency over a three-year observation period. In a one-dimensional poroelastic model of ocean tidal loading this phase lag corresponds to a high-permeability system where pore pressure perturbations at the seafloor rapidly propagate downward from the seafloor interface until they encounter a permeability boundary. Our results suggest that at the Lucky Strike field this tidal pumping is largely restricted to the ~600 m thick extrusive layer (i.e., seismic layer 2A). Under a plausible set of matrix elastic parameters, the ~5.3 h lag between pressure and exit-fluid temperature is consistent with an effective matrix permeability of $\sim 10^{-10}$ m^2 and an average vertical flow velocity of ~0.02 m/s within the extrusive layer. Our results argue against tidal pumping of the entire crustal section between the seafloor and the axial magma chamber (at ~3.4 kmbsf) because this scenario requires unrealistically high effective permeabilities ($\sim 10^{-9}$ m^2) and average vertical flow velocities (~0.15 m/s) over this depth range. Our effective permeability estimate for the extrusive layer is broadly consistent with previous results, and indicates that flow must be channeled in discrete permeable pathways (e.g., faults, fissures) that cut through the extrusive volcanic layer.

1. Introduction

Hydrothermal fluids at mid-ocean ridges (MORs) circulate in a porous, elastic matrix that is periodically loaded by ocean tides. When the medium is loaded, the resultant stress is borne partly by the solid matrix and partly by the interstitial fluid. Tidal loading generates both an instantaneous pressure perturbation with a constant magnitude at all depths and a time-dependent pore pressure perturbation resulting from flow-induced diffusion (Van der Kamp and Gale, 1983). The instantaneous signal is in phase with the ocean tide while the diffusive pressure perturbation cyclically modifies pore pressures and the upwelling fluid velocity at the forcing periods, producing a phase lag between the vertical fluid velocity and the tidal loading function that depends upon the poroelastic parameters of the system, such as the permeability, fluid viscosity, and storage capacity (e.g., Wang and Davis, 1996; Wilcock and McNabb, 1996; Jupp and Schultz, 2004; Crone and Wilcock, 2005). In particular, the poroelastic response is highly sensitive to the matrix permeability, which controls the diffusion rate of pore pressure perturbations, as well as the velocity of the hydrothermal fluids. Thus, if the phase lag between exit-fluid velocity (or temperature) and the tidal loading function at a MOR hydrothermal site can be accurately estimated it should be possible to place meaningful constraints on the permeability of the matrix hosting flow (Jupp and Schultz, 2004; Crone and Wilcock, 2005).

While it is technically very difficult to make time-series measurements of exit-fluid velocity at a deep-sea vent field, it is much simpler to measure fluid temperature, and tidal periodicities are commonly observed in exit-fluid temperature records from hydrothermal vents at MORs (e.g., Tivey et al., 2002; Jupp and Schultz, 2004; Crone and Wilcock, 2005; Scheirer et al., 2006; Sohn, 2007; Larson et al., 2007; Barreyre et al., 2014). These records clearly demonstrate that exit-fluid temperatures are

* Corresponding author at: Woods Hole Oceanographic Institution, Woods Hole, MA, USA. Tel.: +1 (508) 289 3332.
E-mail address: tbarreyre@whoi.edu (T. Barreyre).

http://dx.doi.org/10.1016/j.epsl.2014.09.049
0012-821X/

modulated at a variety of tidal periods (e.g., diurnal, semi-diurnal, etc.), but because bottom currents may also affect exit-fluid temperature measurements (e.g., Tivey et al., 2002) it has not been clear whether the tidal periodicities were induced by poroelastic effects from tidal loading, by tidal currents, or a combination or both. Recently, Barreyre et al. (2014) showed that in the case of Lucky Strike Hydrothermal Field, where tidal loading and bottom currents have been contemporaneously measured with exit-fluid temperatures from multiple vents over a ~3 yr interval, tidal signals in the high-temperature records (>200 °C) are correlated with loading whereas tidal signals in the low-temperature records (<100 °C) are correlated with currents. These results indicate that the poroelastic response to tidal loading can generate observable exit-fluid temperature perturbations, and that these perturbations are most readily observed in high-temperature discharge features where velocities are highest and where measurements can often be made inside a well-developed orifice or vent to shield the sensor from bottom currents.

In this paper, we investigate the feasibility of using the phase lag between exit-fluid temperature and tidal loading to constrain matrix poroelastic parameters using three consecutive years of temperature and pressure data from the LSHF (Barreyre et al., 2014; the temperature data is publicly available – http://dx.doi.org/10.1594/PANGAEA.820343). We find that the high-temperature ($T > 200$ °C) discharge records are strongly correlated with tidal pressure at semi-diurnal periods with a consistent phase lag of ~155° relative to tidal loading (5.3 h, M2 period). We apply these lags to the 1-dimensional poroelastic model of Jupp and Schultz (2004) to obtain crustal permeabilities, and discuss whether or not the diffusive pore pressure perturbations are restricted to the upper crust (~600 m thick extrusive volcanic layer) or extend all the way to the magma chamber at ~3400 m. We conclude by discussing the implications of our results for hydrothermal circulation at deep-sea fields and considering the limitations imposed by our use of a one-dimensional poroelastic model.

2. Phase lag between tidal forcing and exit-fluid thermal response

The MOMAR (Monitoring the Mid-Atlantic Ridge) experiment has measured exit-fluid temperatures at 9 sites at the LSHF since 2009, along with other parameters such as bottom pressure, bottom currents, and seismicity (Ballu et al., 2009; Colaço et al., 2011; Crawford et al., 2013; Barreyre et al., 2014). For this study we use the eight best-quality, high-temperature ($T > 200$ °C) exit-fluid records acquired at four sites between 2009–2012 (Fig. 1, Barreyre et al., 2014) to estimate the phase lag, φ_T, between discharge temperature and bottom pressure at tidal periods. We estimate coherency and phase lag by applying multi-taper (Thomson, 1982) cross-spectral methods with adaptive weighting (Percival and Walden, 1993) to yearlong temperature and pressure records sampled either at 90 s or 24 min intervals. Uncertainties in the phase lag parameter are calculated by jackknifing the independent phase estimates obtained for each of the orthogonal tapers (values are given in Table 1, estimated for all the semi-diurnal tidal constituents).

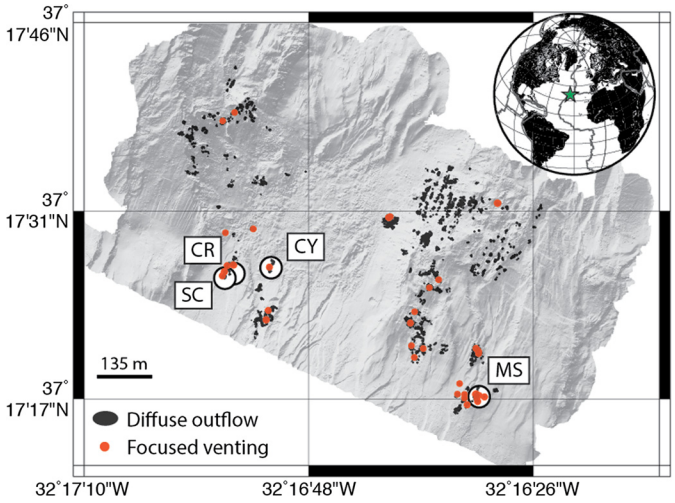

Fig. 1. Shaded relief of the Lucky Strike hydrothermal filed, showing the location of both diffuse outflow (black) and focused venting (red; from Barreyre et al., 2012). The main hydrothermal sites concerned in this study are also indicated: MS, Montsegur; CY, Cypress; CR, Crystal; SC, South Crystal. (For interpretation of the references to color in this figure legend, the reader is referred to the web version of this article.)

All the high-temperature records used in our analysis are highly coherent with bottom pressure at tidal periods (Fig. 2a), with all the semi-diurnal frequencies (i.e., M2, S2, N2 and K2) showing strong and stable levels of coherency and phase lag estimates (Table 1, Fig. 2b). Nevertheless, the highest levels are observed at the lunar, semi-diurnal (M2) frequency (Table 1 and Fig. 2). We thus restrict our phase angle analysis to the M2 frequency to obtain the most robust results. We find that the phase-lag estimates are broadly consistent for different sites across the field and for

Table 1
Coherence, phase lag and errors estimates, at different tidal semi-diurnal frequencies (i.e. M_2, K_2, S_2 and N_2), for different vents and deployments, and for the whole Lucky Strike hydrothermal field. Note that field average phase lag estimates for all the different semi-diurnal constituents are consistent and about the same.

		MS[a]			CR[a]		SC[a]		CY[a]	LSHF[a]
		09–10 HW0007A	10–11 HW0014A	11–12 HW0020B	09–10 HW0006A	11–12 HW0019B	09–10 HN29010	10–11 HW0006B	11–12 HN30001	09–12 All
M2	Coherency (γ^2)	0.85	0.94	0.87	0.81	0.92	0.92	0.72	0.65	–
	Phase lag (φ, °)	**156.6**	**161.5**	**170.2**	**162.8**	**153.8**	**137.9**	**147.2**	**151.4**	**155.2**
	Error (°)[b]	2.5	0.9	1.3	4.1	2.2	1.8	3.5	3.6	**2.5**
K2	Coherency (γ^2)	0.82	0.90	0.79	0.70	0.82	0.77	0.69	0.63	–
	Phase lag (φ, °)	157.2	154.5	167.6	154.6	161.6	147.9	136.4	163.9	**155.5**
	Error (°)[b]	1.8	1.6	2.2	3.6	1.9	2.3	3.1	5	2.7
S2	Coherency (γ^2)	0.81	0.90	0.79	0.42	0.81	0.80	0.58	0.57	–
	Phase lag (φ, °)	157.3	154.6	167.3	151.6	161.4	147.8	134.5	162.6	**154.6**
	Error (°)[b]	2	2.6	2	4	2.1	1.8	5.5	4	3
N2	Coherency (γ^2)	0.79	0.74	0.77	0.30	0.35	0.26	0.46	0.36	–
	Phase lag (φ, °)	146.6	149.4	*188.1*	163.3	160.3	136.7	120.6	128.3	***149.2***
	Error (°)[b]	2.7	2.4	2.5	8.8	6.1	9.5	10.1	8	6.3

[a] See Fig. 1 for location and full name of sites corresponding to the acronyms in this table.
[b] Errors in the phase lag parameter are calculated by jackknifing the independent phase estimates obtained for each of the orthogonal tapers.